Robust dynamical and steady-state entanglement of phonons in the magnetic microsphere

Xiao-Wen Huo, Shi-Ni Yang, Xin-Lei Hei,* Jia-Qiang Chen, Yi-Fan Qiao, Xue-Feng Pan, Xiao-Yu Yao, Jun-Cong Zheng, Yu-Meng Ren, Guo-Yu Shu, and Peng-Bo Li†

Ministry of Education Key Laboratory for Nonequilibrium Synthesis and Modulation of Condensed Matter, Shaanxi Province Key Laboratory of Quantum Information and Quantum Optoelectronic Devices, School of Physics, Xi'an Jiaotong University, Xi'an 710049, China

(Received 9 January 2025; revised 27 June 2025; accepted 21 August 2025; published 22 October 2025)

In the field of quantum information, robust entanglement has received widespread attention. In this work, we investigate the magnon-mediated robust entanglement between the acoustic phonon and the center-of-mass motion (CMM) phonon in a yttrium iron garnet sphere. By analyzing the system's dynamic evolution, we demonstrate that phonon-phonon entanglement, which is robust with respect to the magnon mode, can be generated at a specific moment. Furthermore, we introduce a scheme for generating stable bipartite entanglement that remains robust against varying initial states by utilizing an engineered reservoir. This approach maintains effectiveness even under high dissipation rates of the magnon mode, leveraging the magnon dissipation as a beneficial resource. The approaches we present for generating robust phonon-phonon entanglement not only offer a feasible method for monitoring internal acoustic modes within magnetic systems using easily detectable CMM phonons, but also provide a viable platform for the manipulation and processing of quantum information.

DOI: 10.1103/b6kk-rd74

I. INTRODUCTION

Quantum entanglement, a distinctive phenomenon that arises uniquely in the quantum domain, has attracted increasing attention since its inception [1] and theoretical confirmation [2], particularly after its experimental validation [3]. As a manifestation of the nonlocal nature of quantum mechanics, entanglement has become a crucial resource for quantum computation, quantum information processing, and the transmission of quantum states [4–10]. In addition, realizing the entanglement between distinct quantum systems is essential for exploring and enhancing the benefits of quantum entanglement, as well as broadening its practical applications.

Recently, magnons have garnered growing attention with its abundant modal structures and exceptional tunability [11,12]. Magnons have been extensively studied in spherical [13–22], lumped (thin-film) [23–39], and two-dimensional [40–49] magnetic systems. In particular, spherical yttrium iron garnet (YIG) magnets [17–21], which possess high spin density and low damping rates [50], have enabled the realization of strong coupling between magnons and various other quantum systems, including photons [50–62], phonons [63,64], superconducting qubits [65–72], and solid-state spins [73–75]. Furthermore, within the YIG magnetic sphere, multiple phonon modes exist in addition to magnon modes, such as internal acoustic phonons and center-of-mass motion (CMM) phonons. The magnon-magnon [76–81], magnon-acoustic phonon [82–92], and magnon-CMM phonon [93,94] entanglement in isolated magnetic systems has been realized due to the strong coupling between magnons and these modes. However, direct interactions between acoustic phonons and CMM phonons in isolated magnets are lacking, and thus the methods to achieve entanglement between these two phonon modes remain to be explored. Specifically, realizing the aforementioned bipartite entanglement can provide a feasible phonon-phonon resource for studying entanglement phenomena in isolated magnets, without requiring the involvement of other quantum systems. Additionally, it could offer a promising approach for detecting and modulating the internal acoustic phonons through the easily detectable CMM of magnets. Therefore, investigating the interaction and entanglement between acoustic phonons and CMM phonons in magnets is of paramount importance for exploring novel quantum effects in isolated magnets.

In this work, we propose two distinct approaches to achieve entanglement between the acoustic phonon, arising from the internal degrees of freedom, and the CMM phonon, originating from the external degrees of freedom of a YIG microsphere, mediated by the magnon mode. In the first scheme, we aim to generate a dynamical phonon-phonon entanglement that is fully robust against the magnon mode, periodically, starting from the Heisenberg equation. This implies that the same level of bipartite entanglement can be periodically achieved regardless of the magnon's initial state. In the second approach, we take into account the high dissipation of the magnon mode, demonstrating that the magnon's dissipation can serve as a beneficial resource, facilitating the successful preparation of phonon-phonon entanglement through cooling the Bogoliubov mode composed of two phonons using the reservoir engineering method. This work offers a practicable approach and a promising platform for quantum information

*Contact author: heixinlei@gmail.com
†Contact author: lipengbo@mail.xjtu.edu.cn

Published by the American Physical Society under the terms of the Creative Commons Attribution 4.0 International license. Further distribution of this work must maintain attribution to the author(s) and the published article's title, journal citation, and DOI.

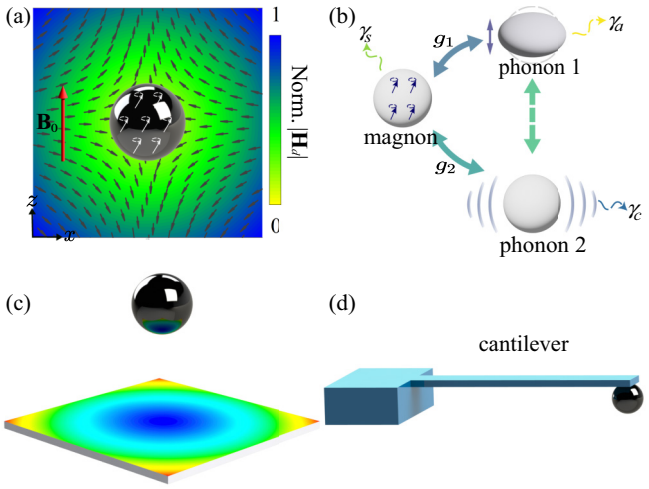


FIG. 1. The theoretical model of our scheme and feasible setups to capture the YIG microsphere. (a) Schematic illustration of a YIG microsphere subjected to a field consisting of a uniformly biased field $\mathbf{B}_0$ (red arrow) along the z direction, and a weak gradient driving field $\mathbf{H}_d$ (shown in the bottom layer with a color gradient) with dark-gray arrows demonstrating the direction of the driving field. (b) Under the appropriate conditions, magnons interact with acoustic phonons (phonon 1) and CMM phonons (phonon 2) with the coupling rates g_1 and g_2, respectively. Through the mediation of magnons, these two types of phonons interact indirectly. γ_s, γ_a, and γ_c represent the damping rates of corresponding modes. (c) Capturing the YIG microsphere in a harmonic potential well. (d) Attaching the YIG microsphere on a cantilever.

processing, representing significant progress toward the generalization of entanglement.

The paper is organized as follows. In Sec. II, we describe the theoretical model under study and present the Hamiltonian of our system. In Sec. III, we discuss how to achieve the robust dynamical entanglement and steady-state entanglement between two phonon modes and show that the resulting entanglement is a manifestation of two-mode squeezing. In Sec. IV, we analyze the experimental feasibility of the proposed schemes. Finally, in Sec. V, we present a discussion of our results.

II. THE SETUP

As illustrated in Fig. 1(a), we consider a YIG microsphere with a radius of 100 nm, placed in a magnetic field composed of a uniform bias field along the z direction and a weak gradient driving field. Through the quantization of the spin waves, displacement field, and the CMM, we derive the magnon Hamiltonian $\hat{H}_s$, acoustic phonon Hamiltonian $\hat{H}_a$, and CMM Hamiltonian $\hat{H}_c$, respectively, for the modes under consideration. The free Hamiltonian of the system is given by

$$\begin{aligned}\hat{H}_0 &= \hat{H}_s + \hat{H}_a + \hat{H}_c \\ &= \hbar\omega_s \hat{s}^\dagger \hat{s} + \hbar\omega_a \hat{a}^\dagger \hat{a} + \hbar\omega_c \hat{c}^\dagger \hat{c},\end{aligned} \tag{1}$$

where ω_s, ω_a, and ω_c are the eigenfrequencies of the magnonic mode, acoustic phononic mode, and center-of-mass motional (CMM) phonon mode under consideration, respectively. The operators $\hat{s}^\dagger(\hat{s})$, $\hat{a}^\dagger(\hat{a})$, and $\hat{c}^\dagger(\hat{c})$ denote the creation (annihilation) operators of the magnon (Kittel mode), acoustic phonon, and the CMM phonon, respectively.

We now consider the interaction between different eigenmodes. The magnon mode can be strongly coupled to the phonon mode within the magnet through magnetoelastic interactions. We describe the interaction between the magnon and the phonon starting from the magnetoelastic energy density,

$$\begin{aligned}U_{\rm mo}(\mathbf{r},t) = \sum_{i,j=x,y,z} &\frac{B_2 + \delta_{ij}(B_1 - B_2)}{M_s^2} \\ &\times M_i(\mathbf{r},t) M_j(\mathbf{r},t) \bar{\varepsilon}_{ij}(\mathbf{r},t).\end{aligned} \tag{2}$$

Here, B_1 and B_2 are the magnetoelastic coefficients of the YIG microsphere, $M_i = \mathbf{e}_i \cdot \mathbf{M}$ denotes the directional components of the magnetization, and $\bar{\varepsilon}_{ij} \equiv (\partial_{r_j} u_i + \partial_{r_i} u_j)/2$ represents the dimensionless strain tensor. The strain tensor is derived from the directional components of the lattice continuous displacement field $\mathbf{u}$. By substituting the quantized magnetization and displacement fields into the above equation and integrating over the volume V_0 of the YIG microsphere, we obtain the magnetoelastic interaction Hamiltonian. In our study, we focus on the Kittel mode, and the mode S_{321} during the S_{v21} phonon family which is the only acoustic phonon family coupled with the Kittel mode. In the small-particle limit (radius $R = 100$ nm), assuming that the Kittel mode is in resonance with the S_{321} phonon mode ($\omega_s = \omega_a$), the interaction Hamiltonian between the magnon and the phonon that we considered under the rotation wave is given by

$$\hat{H}_{\text{s-a}} = \hbar g_1 (\hat{s}\hat{a}^\dagger + \hat{s}^\dagger \hat{a}), \tag{3}$$

where $\hat{s}$ ($\hat{s}^\dagger$) and $\hat{a}$ ($\hat{a}^\dagger$) are the annihilation (creation) operators associated with the magnon mode and the internal acoustic phonon, respectively. The symbol g_1 represents the magnon-phonon coupling rate as defined in Eq. (3).

In addition, the Kittel mode can couple to CMM phonons due to the influence of the gradient driving field. Under the driving magnetic $\mathbf{H}_d(\mathbf{r},t) = (b/\mu_0)[-x\mathbf{e}_x + z\mathbf{e}_z]\cos(\omega_d t)$, with ω_d as the frequency of driving field and b as the gradient parameter in $\mathrm{T\,m^{-1}}$, the magnetic energy of the system increases by

$$\Delta E = -\frac{\mu_0}{2}\int_{V_0} dV \mathbf{M}(\mathbf{r},t)\cdot\mathbf{H}_d(\mathbf{r}+\mathbf{R}_{\rm cm},t), \tag{4}$$

where $\mathbf{R}_{\rm cm}$ is the position vector of its center of mass. Two experimental approaches are proposed to realize gradient fields of the specified form: one involves the region near the center of a zero-bias Ioffe-Pritchard trap, while the other utilizes a quadrupole trap [95–97]. By quantizing this energy shown in Eq. (4), the original Hamiltonian describing the interaction between the Kittel mode and the CMM phonon can be given as

$$\begin{aligned}\hat{H}^o_{\text{s-c}}(t) = \frac{bV_0}{2}\cos(\omega_d t)\Big[&M_k(\hat{s}+\hat{s}^\dagger)\hat{X} - M_s\hat{Z} \\ &+ \sum_{l=0,2,4\ldots}\sum_{m=0,\pm2}\sum_{n} M_{zpf}(L_\beta \hat{s}_\beta + \text{H.c.})\Big],\end{aligned} \tag{5}$$

where $M_k = \sqrt{|\gamma|\hbar M_s/(2V_0)}$ is the zero-point magnetization energy of the Kittel mode with the saturation magnetization M_s and the gyromagnetic ratio γ, and $\hat{X}$ ($\hat{Z}$) represent the

vibrational operators describing the CMM of the YIG microsphere along the x (z) directions. In addition, $\hat{s}_\beta$ in the last term of Eq. (5) represents the magnon modes other than the Kittel mode, and this term is expressed in the form adopted in Ref. [98].

We consider the near-resonance condition $\omega_d \sim \omega_s$, under which both the center-of-mass vibrational mode $\hat{Z}$ and the magnon modes $\hat{s}_\beta$ other than the Kittel mode are far detuned from the drive. As a result, the second and third terms in Eq. (5) become fast oscillating and are neglected under the rotating-wave approximation. By expressing the center-of-mass vibrational operator $\hat{X}$ in terms of the phonon creation (annihilation) operators $\hat{c}^\dagger$ ($\hat{c}$), i.e., $\hat{X} = \sqrt{\hbar/(2\rho V_0 \omega_c)}(\hat{c}^\dagger + \hat{c})$, where ρ is the density of the YIG microsphere, the effective Hamiltonian describing the interaction between the Kittel mode and the CMM phonon can be expressed as

$$\hat{H}_{\text{s-c}}(t) = \hbar G_x \cos(\omega_d t)(\hat{c} + \hat{c}^\dagger)(\hat{s} + \hat{s}^\dagger), \tag{6}$$

with $G_x = (b/4)\sqrt{|\gamma| M_s/(\rho\omega_c)}$.

Thus, the total Hamiltonian of the system can be written as

$$\begin{aligned}\hat{H}_{\text{total}}(t) &= \hat{H}_0 + \hat{H}_{\text{s-a}} + \hat{H}_{\text{s-c}} \\ &= \hbar\omega_s \hat{s}^\dagger \hat{s} + \hbar\omega_a \hat{a}^\dagger \hat{a} + \hbar\omega_c \hat{c}^\dagger \hat{c} + \hbar g_1(\hat{s}\hat{a}^\dagger + \text{H.c.}) \\ &\quad + \hbar G_x \cos(\omega_d t)(\hat{c}^\dagger + \hat{c})(\hat{s}^\dagger + \hat{s}),\end{aligned} \tag{7}$$

where the first term represents the free Hamitonina of the YIG microsphere, the second term corresponds to the interaction Hamiltonian between the Kittel mode and the acoustic phonon, and the last term describes the interaction between the Kittel mode and the CMM phonon. The Hamiltonian in the interaction picture, under the unitary transformation $\hat{U} = \exp[-i(\omega_s \hat{s}^\dagger \hat{s} + \omega_a \hat{a}^\dagger \hat{a} + \omega_c \hat{c}^\dagger \hat{c})t/\hbar]$, is given by

$$\begin{aligned}\hat{H}_{I0} &= \hbar g_1(\hat{s}\hat{a}^\dagger + \hat{s}^\dagger \hat{a}) \\ &\quad + \hbar G_x \cos(\omega_d t)[(\hat{s}^\dagger \hat{c}^\dagger e^{i\omega_+ t} + \hat{s}^\dagger \hat{c} e^{i\omega_- t}) + \text{H.c.}],\end{aligned}$$

with $\omega_\pm = \omega_s \pm \omega_c$.

Assuming the driving field is near sum-frequency resonance with the Kittel mode and the CMM phonon mode ($\omega_d \approx \omega_s + \omega_c$), and applying Euler's formula along with the rotating-wave approximation with the condition $2\omega_c \gg G_x$, we obtain the final interaction Hamiltonian in the form of

$$\hat{H}_I = \hbar g_1(\hat{s}\hat{a}^\dagger + \hat{s}^\dagger \hat{a}) + \hbar g_2(\hat{s}\hat{c} + \hat{s}^\dagger \hat{c}^\dagger), \tag{8}$$

with $g_2 = G_x/2$. The mediation of the magnons enables the coupling between the acoustic phonon and the CMM phonon mode, as depicted in Fig. 1(b).

Furthermore, to capture the YIG microsphere, we consider two experimental mechanisms, as shown in Figs. 1(c) and 1(d), both of which have been successfully implemented in the laboratory. The first mechanism shown in Fig. 1(c) involves levitating the YIG microsphere in a harmonic potential, such as an in-plane zero-bias trapping or the Paul trap [99], which allows for the realization of a high-Q CMM phonon mode. For the other way, one can attach the magnetic sphere to a cantilever [100–105], as illustrated in Fig. 1(d), which is much easier to implement.

III. BIPARTITE ENTANGLEMENT BETWEEN THE ACOUSTIC PHONON AND THE PHONON OF THE CM MOTION AND ITS APPLICATION

A. Robust dynamical entanglement between the acoustic phonon and the phonon of the CM motion

From Eq. (8), the Hamiltonian of the magnetic microsphere, we derive the dynamic equation, i.e., the Hisenberg equation of these modes,

$$\dot{\hat{a}} = -ig_1 \hat{s}, \tag{9a}$$

$$\dot{\hat{c}} = -ig_2 \hat{s}^\dagger, \tag{9b}$$

$$\dot{\hat{s}} = -ig_1 \hat{a} - ig_2 \hat{c}^\dagger. \tag{9c}$$

It is straightforward to obtain that $\ddot{\hat{s}} = (g_2^2 - g_1^2)\hat{s}$, which implies that $\hat{s}$ evolves periodically when $|g_1| > |g_2|$. Assuming that solution is satisfied, we can derive the time evolution of these modes,

$$\begin{aligned}\hat{a}(t) &= -\frac{ig_1}{g}\hat{s}(0)\sin(gt) - \frac{1}{g^2}\left[g_2^2 - g_1^2\cos(gt)\right]\hat{a}(0) \\ &\quad -\frac{g_1 g_2}{g^2}[1 - \cos(gt)]\hat{c}^\dagger(0),\end{aligned} \tag{10a}$$

$$\begin{aligned}\hat{c}(t) &= -\frac{ig_2}{g}\hat{s}^\dagger(0)\sin(gt) + \frac{1}{g^2}\left[g_1^2 - g_2^2\cos(gt)\right]\hat{c}(0) \\ &\quad +\frac{g_1 g_2}{g^2}[1 - \cos(gt)]\hat{a}^\dagger(0),\end{aligned} \tag{10b}$$

$$\hat{s}(t) = \hat{s}(0)\cos(gt) - \frac{i}{g}[g_1 \hat{a}(0) + g_2 \hat{c}^\dagger(0)]\sin(gt), \tag{10c}$$

which show how these three modes become entangled, where $\hat{s}(0)$, $\hat{c}(0)$, and $\hat{a}(0)$ are the initial states of these modes, respectively, and $g = \sqrt{|g_1|^2 - |g_2|^2}$. It is noteworthy that the situation is special at the time $t_n = n\pi/g$, ($n = 1, 3, 5, \ldots$), at which these three modes evolve to

$$\hat{a}(t_n) = -\frac{1}{g^2}\left(g_2^2 + g_1^2\right)\hat{a}(0) - \frac{2g_1 g_2}{g^2}\hat{c}^\dagger(0), \tag{11a}$$

$$\hat{c}(t_n) = \frac{1}{g^2}\left(g_1^2 + g_2^2\right)\hat{c}(0) + \frac{2g_1 g_2}{g^2}\hat{a}^\dagger(0), \tag{11b}$$

$$\hat{s}(t_n) = \hat{s}(0), \tag{11c}$$

which show that the magnon mode becomes decoupled from the other two modes and returns to its initial state, while the other two phonon modes couple only with each other. This means that a bipartite entangled state of phonons which is robust with respect to the magnon's initial state can be prepared at a certain time t_n. Considering further, if we define a squeezing operator $\hat{S}(\xi) = \exp[\xi(\hat{a}\hat{c} - \hat{a}^\dagger \hat{c}^\dagger)]$ with $\xi = \ln[(g_1 + g_2)/(g_1 - g_2)]$ as the squeezing parameter, we can rewrite Eqs. (11a) and (11b) as

$$\hat{a}(t_n) = -\cosh\xi \hat{a}(0) - \sinh\xi \hat{c}^\dagger(0) = -\hat{S}\hat{a}(0)\hat{S}^\dagger, \tag{12a}$$

$$\hat{c}(t_n) = \cosh\xi \hat{c}(0) + \sinh\xi \hat{a}^\dagger(0) = \hat{S}\hat{c}(0)\hat{S}^\dagger, \tag{12b}$$

which represent a two-mode squeezed vacuum state under the initial condition that both phonon modes evolve from the vacuum state. The above discussion has been conducted under ideal conditions. In what follows, we consider the dissipation of the three studied modes to the environment. After

introducing dissipation, the dynamic evolution is modified by the quantum Langevin equation,

$$\dot{\hat{a}} = -ig_1\hat{s} - \frac{\gamma_a}{2}\hat{a} + \sqrt{\gamma_a}\hat{a}_{\rm in}, \tag{13a}$$

$$\dot{\hat{c}} = -ig_1\hat{s}^\dagger - \frac{\gamma_c}{2}\hat{c} + \sqrt{\gamma_c}\hat{c}_{\rm in}, \tag{13b}$$

$$\dot{\hat{s}} = -ig_1\hat{a} - ig_2\hat{c}^\dagger - \frac{\gamma_s}{2}\hat{s} + \sqrt{\gamma_s}\hat{s}_{\rm in}, \tag{13c}$$

where γ_o, $(o = a, c, s)$ represent the corresponding damping rates to the environment for the respective operators. The damping rate γ_o is related to the natural frequency ω_o and quality factor Q_o of the corresponding mode via the relation $\gamma_o = \omega_o/Q_o$. In addition, $\hat{o}_{\rm in}$ are the corresponding noise input operators which satisfy the correlation function,

$$\langle\hat{o}^\dagger_{\rm in}(t)\hat{o}_{\rm in}(t')\rangle = n_o\delta(t-t'), \tag{14a}$$

$$\langle\hat{o}_{\rm in}(t)\hat{o}^\dagger_{\rm in}(t')\rangle = (n_o+1)\delta(t-t'), \tag{14b}$$

where $n_o = [\exp(\hbar\omega_o/k_BT) - 1]^{-1}$ are the corresponding average thermal occupation numbers, with k_B being the Boltzmann constant and T the temperature of the environment. By introducing a set of quadrature operators, $\hat{X}_o = (\hat{o} + \hat{o}^\dagger)/\sqrt{2}$ and $\hat{Y}_o = (\hat{o} - \hat{o}^\dagger)/(i\sqrt{2})$, the quantum Langevin equations can be written in a compact form,

$$\dot{R} = MR + N, \tag{15}$$

where $R = [\hat{X}_c, \hat{Y}_c, \hat{X}_s, \hat{Y}_s, \hat{X}_a, \hat{Y}_a]^T$ and $N = [\sqrt{\gamma_c}\hat{X}_{c_{\rm in}}, \sqrt{\gamma_c}\hat{Y}_{c_{\rm in}}, \sqrt{\gamma_s}\hat{X}_{s_{\rm in}}, \sqrt{\gamma_s}\hat{Y}_{s_{\rm in}}, \sqrt{\gamma_a}\hat{X}_{a_{\rm in}}, \sqrt{\gamma_a}\hat{Y}_{a_{\rm in}}]^T$ are the column vectors of the quadrature operators and noise operators, respectively, for the three modes. Here, the specific form of the coefficient matrix is given by

$$M = \begin{bmatrix} -\frac{\gamma_c}{2} & 0 & 0 & -g_2 & 0 & 0 \\ 0 & -\frac{\gamma_c}{2} & -g_2 & 0 & 0 & 0 \\ 0 & -g_2 & -\frac{\gamma_s}{2} & 0 & 0 & g_1 \\ -g_2 & 0 & 0 & -\frac{\gamma_s}{2} & -g_1 & 0 \\ 0 & 0 & 0 & g_1 & -\frac{\gamma_a}{2} & 0 \\ 0 & 0 & -g_1 & 0 & 0 & -\frac{\gamma_a}{2} \end{bmatrix}. \tag{16}$$

In order to calculate the entanglement between the two phonons mode, we transform the compact form of quantum Langevin equations into a differential equation for the covariance matrix,

$$\dot{V} = MV + VM^T + D, \tag{17}$$

with the order $(\hat{c}, \hat{s}, \hat{a})$, where the matrix element of V is $V_{pq} = \langle R_pR_q + R_qR_p\rangle/2$ [106] and D is the diffusion matrix with $D_{pq}\delta(t-t') = \langle N_p(t)N_q(t') + N_q(t)N_p(t')\rangle/2$ with $p, q = 1, 2, \ldots, 6$. As is evident, Eqs. (13) and (17) are equivalent. This transformation is justified because the covariance matrix captures essential quantum correlations between operators in Gaussian systems—as evidenced by our system's Hamiltonian, which confirms its Gaussian nature. The covariance matrix of the acoustic phonon and CMM phonon subsystem can be formulated as

$$V_{\rm ca} = \begin{bmatrix} \psi_c & \psi_{\rm ca} \\ \psi^T_{\rm ca} & \psi_a \end{bmatrix}, \tag{18}$$

where

$$\psi_c = \begin{bmatrix} V_{11} & V_{12} \\ V_{21} & V_{22} \end{bmatrix}, \quad \psi_a = \begin{bmatrix} V_{55} & V_{56} \\ V_{65} & V_{66} \end{bmatrix}, \quad \psi_{\rm ca} = \begin{bmatrix} V_{15} & V_{16} \\ V_{25} & V_{26} \end{bmatrix}. \tag{19}$$

The degree of entanglement between the two phonons is then quantified by

$$E_N = \max(0, -2\ln\eta), \tag{20}$$

where $\eta = \sqrt{(\Sigma - \sqrt{\Sigma^2 - 4\det V_{\rm ca}})/2}$ is the minimum symplectic eigenvalue with $\Sigma = \det\psi_c + \det\psi_a - 2\det\psi_{\rm ca}$ that includes elements of the covariance matrix V_{pq} [107–109]. The covariance matrix, in turn, captures the essential quantum correlations between the system operators, as previously discussed. This entanglement measure, known as the logarithmic negativity, is widely employed to quantify entanglement in bipartite continuous-variable (CV) systems [110,111]. Specifically, if $\eta < 1$, the system exhibits entanglement; conversely, if $\eta \geqslant 1$, then $E_N = 0$, indicating a separable state.

At the beginning, if the two phonon modes $\hat{a}$ and $\hat{c}$ are prepared in the vacuum state, i.e., $|0_a0_c\rangle$, and the magnon mode $\hat{s}$ is initialized in the Fock state $|n_s^0\rangle$, the covariance matrix at the initial moment can be expressed as

$$V_0 = \begin{bmatrix} \frac{1}{2} & 0 & 0 & 0 & 0 & 0 \\ 0 & \frac{1}{2} & 0 & 0 & 0 & 0 \\ 0 & 0 & \frac{2n_s^0+1}{2} & 0 & 0 & 0 \\ 0 & 0 & 0 & \frac{2n_s^0+1}{2} & 0 & 0 \\ 0 & 0 & 0 & 0 & \frac{1}{2} & 0 \\ 0 & 0 & 0 & 0 & 0 & \frac{1}{2} \end{bmatrix}. \tag{21}$$

By combining Eqs. (17) and (21), through an integrator process, we determine the covariance matrix at any arbitrary time. Furthermore, on the basis of Eq. (20), the time evolution of entanglement is obtained and plotted in Figs. 2(a) and 2(b) for different temperature and initial states of the Kittel mode, respectively. It is apparent that the entanglement evolves periodically and gradually decreases. In Fig. 2(a), the entanglement presents a negative feedback of the increasing of environment temperature at the same point in time. Figure 2(b) illustrates the impact of the initial state of the Kittel mode on the evolution of bipartite entanglement. It is noteworthy that the entanglement remains identical at t_n for different values of n_s^0, which implies that the entanglement is robust with respect to the magnon's initial state at these special times. This consequence is consistent with Eq. (11) and our previous discussion. To gain further insight, we plot the entanglement as a function of the ratio of couple rates $\Theta = g_2/g_1$ in Fig. 2(c), which demonstrate that higher entanglement can be achieved by increasing Θ.

However, when we consider E_N as a function of the magnon's damping rate γ_s to study the inference in Fig. 2(d), the result is not ideal. As depicted in Fig. 2(d), E_N decreases with increasing γ_s for different values of Θ, which indicates that the dynamic scheme discussed earlier becomes less effective under a high magnon's damping rate. This result

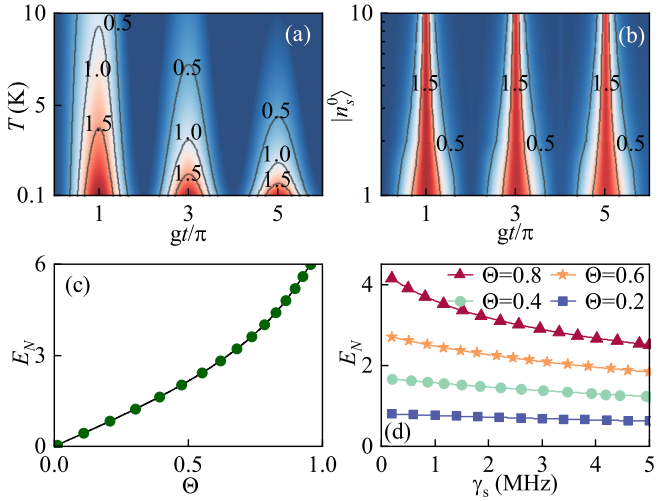


FIG. 2. The contour maps of the time evolution of the dynamics of the entanglement E_N between the acoustic phonon and the CMM phonon vs (a) temperature T and (b) the initial state of the Kittel mode $|n_s^0\rangle$, where the CMM phonon frequency $\omega_c = 2.5g_1$ [112,113]. (c) The maximum value of E_N as a function of Θ, the ratio of couple rates. (d) The dependence of the damping rate of the magnon γ_s on E_N for different values of $\Theta = 0.8, 0.6, 0.4, 0.2$. The parameters used to calculate E_N are $\omega_s = \omega_a$, $\gamma_s = 0.02g_1$, $Q_a = 10^{10}$, and $Q_c = 10^7$.

motivates us to seek another setup for preparing phonon-phonon entanglement with a low Q_s.

B. Robust steady-state entanglement between the acoustic phonon and the phonon of the CM motion

Although a phonon-phonon entangled state can be prepared at specific time, as previously noted, the requirements for preparation, such as magnonic damping rate and truncation of coupling, are somewhat stringent. Therefore, we propose an alternative method of generating the entangled state of the acoustic phonon and CMM phonon, under a high magnonic dissipation condition. Assuming that the damping rate of the magnon mode γ_s is much larger than the coupling rates g_1 and g_2, this high dissipation can be utilized as a favorable condition to cool the Bogoliubov mode, which consists of the acoustic phonon and the CMM phonon, thereby enabling the fabrication of a steady entangled state. To this end, we rewrite the interaction Hamiltonian in Eq. (8) as

$$\hat{H}_I = \sqrt{g_1^2 - g_2^2}\hat{s}^\dagger \left(\frac{g_1}{\sqrt{g_1^2 - g_2^2}}\hat{a} + \frac{g_2}{\sqrt{g_1^2 - g_2^2}}\hat{c}^\dagger \right) + \text{H.c.}, \tag{22}$$

from which we can construct the Bogoliubov modes,

$$\hat{\beta}_1 = \hat{a}\cosh r + \hat{c}^\dagger \sinh r, \tag{23a}$$

$$\hat{\beta}_2 = \hat{c}\cosh r + \hat{a}^\dagger \sinh r, \tag{23b}$$

where $r = \ln[(g_1 + g_2)/(g_1 - g_2)]/2$ and $\tanh r = g_2/g_1$. Then the Hamiltonian in Eq. (22) can be expressed as

$$\hat{H}_I = G(\hat{\beta}_1\hat{s}^\dagger + \hat{\beta}_1^\dagger\hat{s}), \tag{24}$$

in which the Kittel mode $\hat{s}$ and the Bogoliubov mode $\hat{\beta}_1$ are coupled in a beam-splitter interaction form, while the other Bogoliubov mode $\hat{\beta}_2$ decouples with the Hamitonian. In addition, $G = \sqrt{g_1^2 - g_2^2}$ is the coupling rate between the Kittel mode and the Bogoliubov mode $\hat{\beta}_1$. In the interaction picture, the Hamiltonian expressed in Eq. (24) corresponds to a Born-Markov master equation

$$\dot{\rho} = \frac{1}{i\hbar}[\hat{H}_I, \rho] + \sum_{o=a,c,s} \{\gamma_o(n_o + 1)L[\hat{o}]\rho + \gamma_o n_o L[\hat{o}^\dagger]\rho\}, \tag{25}$$

where ρ is the density matrix of the system [114], and the Lindblad operator L is defined as $L[\hat{o}]\rho = \hat{o}\rho\hat{o}^\dagger - \frac{1}{2}\hat{o}^\dagger\hat{o}\rho - \frac{1}{2}\rho\hat{o}^\dagger\hat{o}$. In order to obtain the entangled information, we define another column vector of quadrature operators, $\hat{\mu} = [\hat{X}_{\beta_1}, \hat{Y}_{\beta_1}, \hat{X}_{\beta_2}, \hat{Y}_{\beta_2}, \hat{X}_s, \hat{Y}_s]^T$, where $\hat{X}_x = (\hat{x} + \hat{x}^\dagger)/\sqrt{2}$ and $\hat{Y}_x = (\hat{x} - \hat{x}^\dagger)/(i\sqrt{2})$ are the quadrature operators with $\hat{x} \in \{\hat{\beta}_1, \hat{\beta}_2, \hat{s}\}$, to write the master equation in matrix form. First, the Hamiltonian in Eq. (24) can be expressed as

$$\hat{H}_I = \tfrac{1}{2}\hat{\mu}^\dagger S\hat{\mu}, \tag{26}$$

where

$$S = \begin{bmatrix} 0 & 0 & 0 & 0 & G & 0 \\ 0 & 0 & 0 & 0 & 0 & G \\ 0 & 0 & 0 & 0 & 0 & 0 \\ 0 & 0 & 0 & 0 & 0 & 0 \\ G & 0 & 0 & 0 & 0 & 0 \\ 0 & G & 0 & 0 & 0 & 0 \end{bmatrix}. \tag{27}$$

Afterward, based on the definition of the Lindblad operator, we take the damping rates and the correlation functions $n_o + 1, n_o$ into account in order to matrixize L. It is easy to deduce that

$$\sqrt{\gamma_o(n_o + 1)}\hat{o} = c_o^T\hat{\mu}, \tag{28a}$$

$$\sqrt{\gamma_o n_o}\hat{o}^\dagger = c_{o'}^T\hat{\mu}, \tag{28b}$$

where c_o^T and $c_{o'}^T$ are column vectors of the matrix $C = [c_a^T, c_{a'}^T, c_c^T, c_{c'}^T, c_s^T, c_{s'}^T]$. Combining Eqs. (25), (26), and (28), the differential equation for the covariance matrix σ with matrix elements $\sigma_{pq} = \langle\hat{\mu}_p\hat{\mu}_q + \hat{\mu}_q\hat{\mu}_p\rangle/2$ can be written as

$$\dot{\sigma} = A\sigma + \sigma A^T + D, \tag{29}$$

where $A = \Omega[S + \text{Im}(C^T C)]$ and $D = \Omega\text{Re}(C^T C)\Omega^T$ with $\Omega = \oplus_{k=1}^3 \Phi_k$ is a symplectic matrix [115]. When the system evolves to a steady state, Eq. (29), given by

$$A\sigma^s + \sigma^s A^T = -D, \tag{30}$$

takes the form of a Lyapunov equation, where σ^s is the covariance matrix in the steady state [101,116–118]. Therefore, the condition for the system to reach a steady state is that the real parts of the eigenvalues of A, i.e., the coefficient matrix of the Lyapunov equation, must be negative. In Fig. 3(a), we show the maximum real part of the eigenvalue of A as a function of the ratio between coupling rate $\Theta = g_2/g_1$ ranging from 0 to 1, with the parameters of $\omega_s = \omega_a$, $Q_a = 5 \times 10^{10}$, $Q_c = 10^8$, and $\gamma_s/G = 10$ at $T = 0.1$ K. It is clear that the maximum real part of the eigenvalue is monotonic with Θ, transitioning from

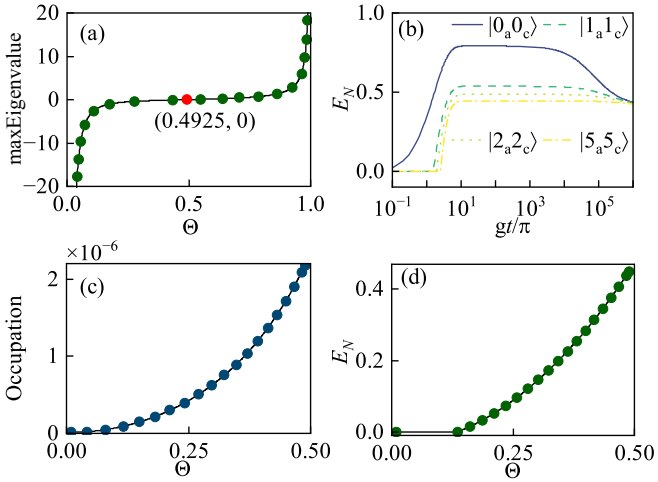


FIG. 3. (a) The maximum value of the real part of eigenvalues of matrix A vs the coupling rate ratio Θ. (b) The time evolution of the dynamics of the entanglement E_N between the acoustic phonon and CMM phonon, with two phonons initially in states $|0_a0_c\rangle$, $|1_a1_c\rangle$, $|2_a2_c\rangle$, and $|5_a5_c\rangle$. (c) The occupation of the Bogoliubov mode β_1 defined as $\langle\hat{\beta}_1^\dagger\hat{\beta}_1\rangle$, as a function of Θ. (d) The influence of Θ on E_N in the steady state. The parameters are $\omega_s = \omega_a$, $\gamma_s/G = 10$, $Q_a = 5\times10^{10}$, $Q_c = 10^8$, and $g_1/2\pi = 9$ MHz at $T = 0.1$ K.

negative to positive around Θ = 0.49, as shown in Fig. 3(a). That means the system can evolve to a steady state for Θ in the range from 0 to 0.49. To verify this, we show the bipartite entanglement versus time in Fig. 3(b) for phonon modes with different initial states, at Θ = 0.49 (satisfying the steady-state condition). As illustrated in Fig. 3(b), the bipartite entanglement resulting from different initial Fock states eventually stabilizes to the same value after a prolonged quasi-steady-state period [119], indicating that the prepared entangled state is robust against the phonons' initial states. Furthermore, we investigate whether the Bogoliubov mode $\hat{\beta}_1$ is cooled to its ground state by plotting the steady occupation number of $\hat{\beta}_1$ as the function of Θ in the range from 0 to 0.49. It is noteworthy that the relationship between the occupation number of $\hat{\beta}_1$ mode and the matrix element is

$$\langle\hat{\beta}_1^\dagger\hat{\beta}_1\rangle = \tfrac{1}{2}\left(\sigma_{11}^s + \sigma_{22}^s\right) - \tfrac{1}{2}. \tag{31}$$

The occupation is far less than 1, as illustrated in Fig. 3(c), which means there is negligible excitation of $\hat{\beta}_1$ and it is in the ground state. To move forward a single step, we present the bipartite entanglement as a function of Θ in Fig. 3(d), with the entanglement quantified by the logarithmic negativity revealed in Eq. (20). The entanglement increases with increasing Θ, as seen in Fig. 3(d). This trend is similar to the result obtained from the dynamic entanglement in Fig. 2(c). However, this approach can prepare a steady entangled state which can persistently exist even under a high magnonic damping rate. Furthermore, although the degree of entanglement obtained by this method is lower than that obtained by the first method, it still could reach values of $E_N > 0.3$ in certain regions, which are comparable to those reported in recent studies of continuous-variable entanglement [111,120,121].

To illustrate the dependence of the bipartite entanglement on temperature, we present the variation of entanglement with

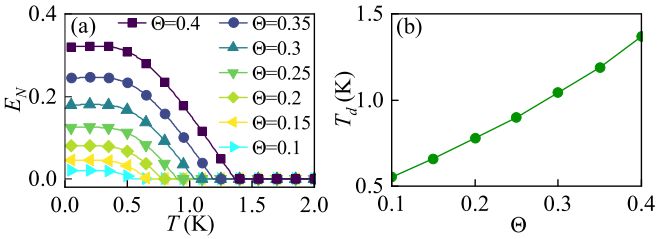


FIG. 4. (a) E_N as a function of temperature T for Θ = 0.1, 0.15, 0.2, 0.25, 0.3, 0.35, 0.4. (b) The relationship between the temperature T_d at which entanglement disappears and Θ. The parameters used here are similar to those in Fig. 3.

T for different values of Θ in Fig. 4(a). At the same temperature, a higher Θ corresponds to a higher entanglement, as shown in Fig. 4(a), which is in full agreement with the conclusion derived from Fig. 3(d). However, at the same Θ, as the temperature increases, the entanglement gradually decreases and eventually disappears. To provide more details, we plot the temperature T_d at which the entanglement disappears as a function of Θ in Fig. 4(b). The results indicate that within the limits of the stable condition, a higher coupling rate ratio can diminish the temperature requirement in the laboratory experiments.

C. Entanglement as a manifestation of two-mode squeezing

Previous studies have shown that depending on the magnetic dissipation rate γ_s, both dynamic and steady-state entanglement can occur between the acoustic phonon and the CMM phonon. This entanglement originates from the effective two-mode squeezing of the phonons and is the manifestation of the two-mode squeezing. Below, we demonstrate this through analysis and numerical simulations.

We introduce two orthogonal quadrature operators, $\hat{X}_1$ and $\hat{X}_2$, defined explicitly as

$$\hat{X}_1 = \frac{\sqrt{2}}{4}(\hat{a} + \hat{a}^\dagger + \hat{c} + \hat{c}^\dagger), \tag{32a}$$

$$\hat{X}_2 = \frac{\sqrt{2}}{4}(\hat{a} - \hat{a}^\dagger + \hat{c} - \hat{c}^\dagger). \tag{32b}$$

As the standard deviations ΔX_1 and ΔX_2 of these operators ($\hat{X}_1$ and $\hat{X}_2$) obey the uncertainty relation

$$(\Delta X_1)(\Delta X_2) \geqslant \tfrac{1}{4}, \tag{33}$$

their variance V_{X_1} and V_{X_2} also satisfy the associated uncertainty relation,

$$\left(V_{X_1}\right)\left(V_{X_2}\right) \geqslant \tfrac{1}{16}. \tag{34}$$

In the absence of squeezing, both variances are equal, i.e., $V_{X_1} = V_{X_2} = 0.25$. When fluctuations in a specific quadrature, such as $\hat{X}_1$, are suppressed, the corresponding variance V_{X_1} becomes less than 0.25. Conversely, the orthogonal quadrature $\hat{X}_2$ becomes antisqueezed, resulting in $V_{X_2} > 0.25$.

The time evolution of V_{X_1} and V_{X_2} during entanglement preparation using the two aforementioned methods is shown in Fig. 5. The parameters are consistent with those used in the entanglement generation process and are detailed in the figure caption. In both scenarios, the system is initialized in the

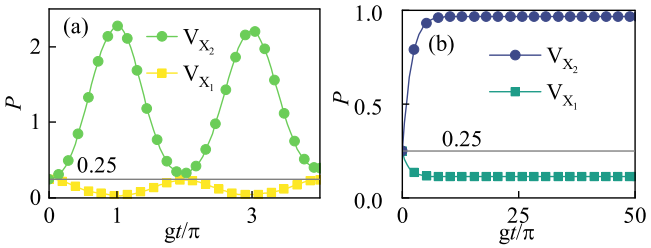


FIG. 5. Time evolution of the variances V_{X_1} and V_{X_2} of the orthogonal quadrature operators $\hat{X}_1$ and $\hat{X}_2$ for two modes $\hat{a}$ (acoustic phonon) and $\hat{c}$ (CMM phonon), during entanglement generation via the two proposed methods. The vertical axis P represents the value of variances V_{X_1} and V_{X_2}. All three modes $\hat{s}$, $\hat{a}$, and $\hat{c}$ are initially prepared in the vacuum state at $T = 0.1$ K. (a) The time evolution of two variances during the dynamically generated entanglement between $\hat{a}$ and $\hat{c}$. Parameters: $\gamma_s = 0.02g_1$, $Q_a = 10^{10}$, and $Q_c = 10^7$. (b) The time evolution of two variances during the generating of steady-state entanglement between $\hat{a}$ and $\hat{c}$. The parameters are $\gamma_s/G = 10$, $Q_a = 5 \times 10^{10}$, and $Q_c = 10^8$.

vacuum state. Figure 5(a) illustrates the time evolution of the variances corresponding to dynamical entanglement. V_{X_1} remains below 0.25 and exhibits periodic oscillations, indicating periodic squeezing in the $\hat{X}_1$ quadrature. This behavior is consistent with the trend of E_N in Figs. 2(a) and 2(b), showing that squeezing in the $\hat{X}_1$ quadrature occurs whenever entanglement is present. Figure 5(b) shows the variances associated with the steady-state entanglement as a function of time. V_{X_1} gradually decreases from 0.25 and stabilizes, indicating that the system can reaches a steady squeezed state. Comparing the blue line in Fig. 3(b), where the system is also initialized in the vacuum state, we can also observe a close correspondence between the entanglement and squeezing behaviors. Figure 5 demonstrates that both the dynamical and steady-state entanglement arise as a manifestation of two-mode phonon squeezing.

It is worth noting that since squeezing plays a fundamental role in enhancing quantum metrology, the squeezing achieved in the $\hat{X}_1$ quadrature by our model can surpass the standard quantum limit when measurements are performed along the the same quadrature. Notably, the steady-state entanglement obtained via the second method corresponds to a two-mode squeezed steady state, indicating that such steady-state preparation can significantly relax the timing requirements in quantum metrology experiments. Specifically, due to the involvement of the CMM phonon mode—sensitive to external forces and magnetic fields—our model enables high-precision sensing of these physical quantities, surpassing the standard quantum limit.

IV. EXPERIMENTAL FEASIBILITY

In this section, we demonstrate the feasibility of entangling the acoustic phonon with the CMM phonon of the magnetic sphere in the above two schemes that we proposed, by means of comparing the used parameters with those from state-of-the-art correlation experiments. The micromagnet we chose is a YIG microsphere with mass density $\rho = 5170\ \mathrm{kg\,m^{-3}}$, saturation magnetization $M_s = 5.87 \times 10^5\ \mathrm{A\,m^{-1}}$, and the magnetoelastic coefficients $B_1 = 3.48 \times 10^5\ \mathrm{J\,m^{-3}}$, $B_2 = 6.4 \times 10^5\ \mathrm{J\,m^{-3}}$ [122]. The quality factor of the acoustic phonon modes in such a YIG sphere can reach values as high as 5×10^{10}. In order to take the CMM phonons into account, one can levitate the magnetic sphere in a harmonic potential well to achieve a high degree of isolation between the magnet and its environment. This isolation is reflected in the quality factor of the magnet's center of mass, which can be up to 10^7-10^8, as experimentally achieved [74,94,96,123–126].

Additionally, the acoustic phonon mode that we chose to couple with the Kittel mode is S_{321}, whose eigenfrequency is $\omega_a = 5.8 \times 10^3 g_1$ with $g_1/2\pi = 9$ MHz, calculated using the eigenfrequency equation with the radius $R = 100$ nm as given in Ref. [98]. Under this consideration, the bias magnetic field required to modulate the eigenfrequency of the Kittel mode into resonance with the S_{321} mode is calculated to be 1.86 T. Furthermore, to implement the coupling between the Kittel mode and the CMM phonon mode, we apply a time-dependent cosine-modulated weak gradient driving magnetic field with frequency $\omega_d/2\pi \sim$ GHz and the gradient $b = 10^5\ \mathrm{T\,m^{-1}}$. This field is in near sum-frequency resonance with both the Kittel mode and the CMM phonon mode, and it is weak enough to have a negligible effect on the Kittel mode [98].

For the first protocol, the damping rate of the magnon mode we use is $\gamma_s = 0.02g_1$ [127] which is smaller than the coupling rates in most cases [128–130]. For the second approach, we investigate the scenario with a high magnon damping, i.e., $\gamma_s/G = 10$, corresponding to $\gamma_s/2\pi$ being below 90 MHz, a regime that is readily accessible in current experiments [131]. Moreover, at an environment of $T = 0.1$ K [132], the mean thermal occupations of the Kittel mode and acoustic phonon mode are $n_s = n_a \approx 2 \times 10^{-11}$, much less than 1.

V. CONCLUSION

To summarize, we propose two distinct approaches to generate bipartite entanglement between the acoustic phonon and the CMM phonon modes of a YIG microsphere, which do not directly interact. The entanglement between the acoustic phonon and CMM phonon is achieved through the mediation of the magnon (Kittel mode). In the first approach, we prepare the acoustic phonon and the CMM phonon entanglement that is robust against the magnon's initial state, leveraging strong coupling between the Kittel mode and both phonons. In the second scheme, we utilize the dissipation of the Kittel mode as a resource for reservoir engineering, enabling the construction of bipartite entanglement under the condition that the damping rate of the Kittel mode far exceeds its coupling rates with these two types of phonons. Importantly, the entanglement generated via the second method is robust with respect to the initial states of both phonons. Moreover, we have shown that the entanglement achieved in our schemes corresponds to two-mode squeezed states of the acoustic and CMM phonons, enabling high-precision sensing of physical quantities beyond the standard quantum limit, and thus can be applied to quantum metrology. Therefore, the bipartite entanglement achieved here provides a promising resource for quantum metrology.

ACKNOWLEDGMENTS

P.-B.L. is supported by the National Natural Science Foundation of China under Grants No. W2411002 and No. 12375018. X.-L.H. is supported by the Young Scientists Fund of the National Natural Science Foundation of China under Grant No. 12505029, the China Postdoctoral Science Foundation under Grant No. 2025M773347 and the Fundamental Research Funds for the Central Universities of Ministry of Education of China under Grant No. xzy012025086. X.-F.P. is supported by the National Natural Science Foundation of China under Grant No. 124B2091.

DATA AVAILABILITY

The data that support the findings of this article are available from the authors upon reasonable request.

[1] A. Einstein, B. Podolsky, and N. Rosen, Can quantum-mechanical description of physical reality be considered complete? Phys. Rev. **47**, 777 (1935).

[2] J. S. Bell, On the Einstein Podolsky Rosen paradox, Phys. Phys. Fiz. **1**, 195 (1964).

[3] A. Aspect, P. Grangier, and G. Roger, Experimental tests of realistic local theories via Bell's theorem, Phys. Rev. Lett. **47**, 460 (1981).

[4] M. Dalmonte, V. Eisler, M. Falconi, and B. Vermersch, Entanglement hamiltonians: From field theory to lattice models and experiments, Ann. Phys. **534**, 2200064 (2022).

[5] L. Amico, R. Fazio, A. Osterloh, and V. Vedral, Entanglement in many-body systems, Rev. Mod. Phys. **80**, 517 (2008).

[6] J.-W. Pan, Z.-B. Chen, C.-Y. Lu, H. Weinfurter, A. Zeilinger, and M. Żukowski, Multiphoton entanglement and interferometry, Rev. Mod. Phys. **84**, 777 (2012).

[7] X.-M. Hu, Y. Guo, B.-H. Liu, C.-F. Li, and G.-C. Guo, Progress in quantum teleportation, Nat. Rev. Phys. **5**, 339 (2023).

[8] R. Horodecki, P. Horodecki, M. Horodecki, and K. Horodecki, Quantum entanglement, Rev. Mod. Phys. **81**, 865 (2009).

[9] J. P. Covey, H. Weinfurter, and H. Bernien, Quantum networks with neutral atom processing nodes, npj Quantum Inf. **9**, 90 (2023).

[10] H. Yu, A. O. Govorov, H.-Z. Song, and Z. Wang, Time-encoded photonic quantum states: Generation, processing, and applications, Appl. Phys. Rev. **11**, 041318 (2024).

[11] H. Song, S. Hao, Q. Liu, S. Fu, and X.-Z. Wang, Field-tunable Dyakonov surface magnon polaritons in antiferromagnets, J. Appl. Phys. **135**, 083906 (2024).

[12] L. R. Walker, Magnetostatic modes in ferromagnetic resonance, Phys. Rev. **105**, 390 (1957).

[13] V. A. S. V. Bittencourt, C. A. Potts, Y. Huang, J. P. Davis, and S. Viola Kusminskiy, Magnomechanical backaction corrections due to coupling to higher-order Walker modes and Kerr nonlinearities, Phys. Rev. B **107**, 144411 (2023).

[14] J. Bourhill, W. Yu, V. Vlaminck, G. E. W. Bauer, G. Ruoso, and V. Castel, Generation of circulating cavity magnon polaritons, Phys. Rev. Appl. **19**, 014030 (2023).

[15] A. Kani, F. Quijandría, and J. Twamley, Magnonic Einstein–de Haas effect: Ultrafast rotation of magnonic microspheres, Phys. Rev. Lett. **129**, 257201 (2022).

[16] D. Kong, J. Xu, and F. Wang, Nonreciprocal entanglement of ferrimagnetic magnons and nitrogen-vacancy-center ensembles by Kerr nonlinearity, Phys. Rev. Appl. **21**, 034061 (2024).

[17] X.-F. Pan, P.-B. Li, X.-L. Hei, X. Zhang, M. Mochizuki, F.-L. Li, and F. Nori, Magnon-skyrmion hybrid quantum systems: Tailoring interactions via magnons, Phys. Rev. Lett. **132**, 193601 (2024).

[18] J. W. Rao, B. Yao, C. Y. Wang, C. Zhang, T. Yu, and W. Lu, Unveiling a pump-induced magnon mode via its strong interaction with Walker modes, Phys. Rev. Lett. **130**, 046705 (2023).

[19] J. Rao, C. Y. Wang, B. Yao, Z. J. Chen, K. X. Zhao, and W. Lu, Meterscale strong coupling between magnons and photons, Phys. Rev. Lett. **131**, 106702 (2023).

[20] D. Xu, X.-K. Gu, H.-K. Li, Y.-C. Weng, Y.-P. Wang, J. Li, H. Wang, S.-Y. Zhu, and J. Q. You, Quantum control of a single magnon in a macroscopic spin system, Phys. Rev. Lett. **130**, 193603 (2023).

[21] G.-T. Xu, M. Zhang, Y. Wang, Z. Shen, G.-C. Guo, and C.-H. Dong, Magnonic frequency comb in the magnomechanical resonator, Phys. Rev. Lett. **131**, 243601 (2023).

[22] G.-Q. Zhang, Y. Wang, and W. Xiong, Detection sensitivity enhancement of magnon Kerr nonlinearity in cavity magnonics induced by coherent perfect absorption, Phys. Rev. B **107**, 064417 (2023).

[23] R. E. Arias, Spin-wave modes of ferromagnetic films, Phys. Rev. B **94**, 134408 (2016).

[24] K. Baumgaertl and D. Grundler, Reversal of nanomagnets by propagating magnons in ferrimagnetic yttrium iron garnet enabling nonvolatile magnon memory, Nat. Commun. **14**, 1490 (2023).

[25] A. D. Boardman and S. A. Nikitov, Three- and four-magnon decay of nonlinear surface magnetostatic waves in thin ferromagnetic films, Phys. Rev. B **38**, 11444 (1988).

[26] L. J. Cornelissen, J. Liu, R. A. Duine, J. B. Youssef, and B. J. van Wees, Long-distance transport of magnon spin information in a magnetic insulator at room temperature, Nat. Phys. **11**, 1022 (2015).

[27] J. Ding, C. Liu, Y. Zhang, U. Erugu, Z. Quan, R. Yu, E. McCollum, S. Mo, S. Yang, H. Ding, X. Xu, J. Tang, X. Yang, and M. Wu, Nanometer-thick yttrium iron garnet films with perpendicular anisotropy and low damping, Phys. Rev. Appl. **14**, 014017 (2020).

[28] T. Frostad, P. Pirro, A. A. Serga, B. Hillebrands, A. Brataas, and A. Qaiumzadeh, Anisotropy-assisted magnon condensation in ferromagnetic thin films, Phys. Rev. Res. **6**, L012011 (2024).

[29] S. S. Gaur and E. E. Marinero, Emergent magnonic materials: Challenges and opportunities, Materials **16**, 6299 (2023).

[30] J. M. Lee, T. Kottos, and B. Shapiro, Macroscopic magnetic structures with balanced gain and loss, Phys. Rev. B **91**, 094416 (2015).

[31] C. L. Ordóñez Romero, B. A. Kalinikos, P. Krivosik, W. Tong, P. Kabos, and C. E. Patton, Three-magnon splitting and confluence processes for spin-wave excitations in yttrium iron garnet films: Wave vector selective Brillouin light scattering measurements and analysis, Phys. Rev. B **79**, 144428 (2009).

[32] H. Qin, G.-J. Both, S. J. Hämäläinen, L. Yao, and S. van Dijken, Low-loss YIG-based magnonic crystals with large tunable bandgaps, Nat. Commun. **9**, 5445 (2018).

[33] A. Rückriegel, P. Kopietz, D. A. Bozhko, A. A. Serga, and B. Hillebrands, Magnetoelastic modes and lifetime of magnons in thin yttrium iron garnet films, Phys. Rev. B **89**, 184413 (2014).

[34] L. Sheng, M. Elyasi, J. Chen, W. He, Y. Wang, H. Wang, H. Feng, Y. Zhang, I. Medlej, S. Liu, W. Jiang, X. Han, D. Yu, J.-P. Ansermet, G. E. W. Bauer, and H. Yu, Nonlocal detection of interlayer three-magnon coupling, Phys. Rev. Lett. **130**, 046701 (2023).

[35] T. Srivastava, H. Merbouche, I. Ngouagnia Yemeli, N. Beaulieu, J. Ben Youssef, M. Muñoz, P. Che, P. Bortolotti, V. Cros, O. Klein, S. Sangiao, J. M. De Teresa, S. O. Demokritov, V. E. Demidov, A. Anane, C. Serpico, M. d'Aquino, and G. de Loubens, Identification of a large number of spin-wave eigenmodes excited by parametric pumping in yttrium iron garnet microdisks, Phys. Rev. Appl. **19**, 064078 (2023).

[36] L. Wang, Z. Lu, X. Zhao, W. Zhang, Y. Chen, Y. Tian, S. Yan, L. Bai, and M. Harder, Magnetization coupling in a YIG/GGG structure, Phys. Rev. B **102**, 144428 (2020).

[37] Z. Wang, Y. Sun, M. Wu, V. Tiberkevich, and A. Slavin, Control of spin waves in a thin film ferromagnetic insulator through interfacial spin scattering, Phys. Rev. Lett. **107**, 146602 (2011).

[38] H. Yang, C. Wang, T. Yu, Y. Cao, and P. Yan, Antiferromagnetism emerging in a ferromagnet with gain, Phys. Rev. Lett. **121**, 197201 (2018).

[39] T. Yu, H. Yang, L. Song, P. Yan, and Y. Cao, Higher-order exceptional points in ferromagnetic trilayers, Phys. Rev. B **101**, 144414 (2020).

[40] J. Aftergood and S. Takei, Conductivity enhancement in a diffusive Fermi liquid due to Bose-Einstein condensation of magnons, Phys. Rev. Lett. **130**, 086702 (2023).

[41] A. T. Costa, M. I. Vasilevskiy, J. Fernández-Rossier, and N. M. R. Peres, Strongly coupled magnon-plasmon polaritons in graphene-two-dimensional ferromagnet heterostructures, Nano Lett. **23**, 4510 (2023).

[42] J. Cui, E. V. n. Boström, M. Ozerov, F. Wu, Q. Jiang, J.-H. Chu, C. Li, F. Liu, X. Xu, A. Rubio, and Q. Zhang, Chirality selective magnon-phonon hybridization and magnon-induced chiral phonons in a layered zigzag antiferromagnet, Nat. Commun. **14**, 3396 (2023).

[43] C. Liu, Z. Li, J. Hu, H. Duan, C. Wang, L. Cai, S. Feng, Y. Wang, R. Liu, D. Hou, C. Liu, R. Zhang, L. Zhu, Y. Niu, A. A. Zakharov, Z. Sheng, and W. Yan, Probing the Néel-type antiferromagnetic order and coherent magnon–exciton coupling in van der Waals VPS_3, Adv. Mater. **35**, 2300247 (2023).

[44] J. Luo, S. Li, Z. Ye, R. Xu, H. Yan, J. Zhang, G. Ye, L. Chen, D. Hu, X. Teng, W. A. Smith, B. I. Yakobson, P. Dai, A. H. Nevidomskyy, R. He, and H. Zhu, Evidence for topological magnon-phonon hybridization in a 2D antiferromagnet down to the monolayer limit, Nano Lett. **23**, 2023 (2023).

[45] A. Mitra, A. Corticelli, P. Ribeiro, and P. A. McClarty, Magnon interference tunneling spectroscopy as a probe of 2D magnetism, Phys. Rev. Lett. **130**, 066701 (2023).

[46] N. Vidal-Silva, F. J. Peña, R. E. Troncoso, and P. Vargas, Magnonic Otto thermal machine, Phys. Rev. Res. **6**, 033164 (2024).

[47] E. Viñas Boström, T. S. Parvini, J. W. McIver, A. Rubio, S. V. Kusminskiy, and M. A. Sentef, Direct optical probe of magnon topology in two-dimensional quantum magnets, Phys. Rev. Lett. **130**, 026701 (2023).

[48] K. Wang, K. Ren, Y. Hou, Y. Cheng, and G. Zhang, Magnon–phonon coupling: From fundamental physics to applications, Phys. Chem. Chem. Phys. **25**, 21802 (2023).

[49] B. Wei, J.-J. Zhu, Y. Song, and K. Chang, Strain-engineered magnon states in two-dimensional ferromagnetic monolayers, Phys. Rev. Res. **6**, 013210 (2024).

[50] J. Bourhill, N. Kostylev, M. Goryachev, D. L. Creedon, and M. E. Tobar, Ultrahigh cooperativity interactions between magnons and resonant photons in a yig sphere, Phys. Rev. B **93**, 144420 (2016).

[51] Y.-J. Ding and Y. Xiao, Eigenstates and temporal dynamics in cavity optomagnonics, Chin. Phys. B **32**, 107601 (2023).

[52] Y. Fang, W. Zhong, G. Cheng, and A. Chen, Magnon-photon cross-correlations via optical nonlinearity in cavity magnonical system, Opt. Express **31**, 27381 (2023).

[53] X. Jiang, S. Tang, and S. Li, Kerr-nonlinearity-triggered nonclassicality of magnons in a photon-magnon coupling system, Photonics **9**, 681 (2022).

[54] N. Kostylev, M. Goryachev, and M. E. Tobar, Superstrong coupling of a microwave cavity to yttrium iron garnet magnons, Appl. Phys. Lett. **108**, 062402 (2016).

[55] A. B. A. Mohamed and H. Eleuch, Dynamics of two magnons coupled to an open microwave cavity: Local quantum Fisher- and local skew-information coherence, Eur. Phys. J. Plus **137**, 853 (2022).

[56] H. Pan, Y. Yang, Z. H. An, and C.-M. Hu, Bistability in dissipatively coupled cavity magnonics, Phys. Rev. B **106**, 054425 (2022).

[57] S. Sharma, Y. M. Blanter, and G. E. W. Bauer, Light scattering by magnons in whispering gallery mode cavities, Phys. Rev. B **96**, 094412 (2017).

[58] S. Verma, A. Maurya, R. Singh, and B. Bhoi, Control of photon-magnon coupling in a planar hybrid configuration, J. Supercond. Novel Magn. **37**, 1163 (2024).

[59] D. Wagle, A. Rai, M. T. Kaffash, and M. B. Jungfleisch, Controlling magnon-photon coupling in a planar geometry, J. Phys. Mater. **7**, 025005 (2024).

[60] Y.-P. Wang, G.-Q. Zhang, D. Zhang, T.-F. Li, C.-M. Hu, and J. Q. You, Bistability of cavity magnon polaritons, Phys. Rev. Lett. **120**, 057202 (2018).

[61] D. Zhang, X.-M. Wang, T.-F. Li, X.-Q. Luo, W. Wu, F. Nori, and J. Q. You, Cavity quantum electrodynamics with ferromagnetic magnons in a small yttrium-iron-garnet sphere, npj Quantum Inf. **1**, 15014 (2015).

[62] X. Zhang, C.-L. Zou, L. Jiang, and H. X. Tang, Strongly coupled magnons and cavity microwave photons, Phys. Rev. Lett. **113**, 156401 (2014).

[63] Y. Li, C. Zhao, W. Zhang, A. Hoffmann, and V. Novosad, Advances in coherent coupling between magnons and acoustic phonons, APL Mater. **9**, 060902 (2021).

[64] J. Li, S.-Y. Zhu, and G. S. Agarwal, Squeezed states of magnons and phonons in cavity magnomechanics, Phys. Rev. A **99**, 021801 (2019).

[65] V. Karanikolas, T. Kuroda, and J. I. Inoue, Magnon-mediated spin entanglement in the strong-coupling regime, Phys. Rev. Res. **4**, 043180 (2022).

[66] D. Lachance-Quirion, S. P. Wolski, Y. Tabuchi, S. Kono, K. Usami, and Y. Nakamura, Entanglement-based single-shot detection of a single magnon with a superconducting qubit, Science **367**, 425 (2020).

[67] C.-X. Ning and M. Yin, Entangling magnon and superconducting qubit by using a two-mode squeezed-vacuum microwave field, J. Opt. Soc. Am. B **38**, 3020 (2021).

[68] M. Setodeh Kheirabady, M. Tavassoly, and S. Salimian, Collapse-revival and stability of magnon-superconducting qubit entanglement in a tripartite hybrid cavity system, Opt. **283**, 170870 (2023).

[69] Y. Tabuchi, S. Ishino, A. Noguchi, T. Ishikawa, R. Yamazaki, K. Usami, and Y. Nakamura, Coherent coupling between a ferromagnetic magnon and a superconducting qubit, Science **349**, 405 (2015).

[70] Y. Tabuchi, S. Ishino, A. Noguchi, T. Ishikawa, R. Yamazaki, K. Usami, and Y. Nakamura, Quantum magnonics: The magnon meets the superconducting qubit, C. R. Phys. **17**, 729 (2016).

[71] S. P. Wolski, D. Lachance-Quirion, Y. Tabuchi, S. Kono, A. Noguchi, K. Usami, and Y. Nakamura, Dissipation-based quantum sensing of magnons with a superconducting qubit, Phys. Rev. Lett. **125**, 117701 (2020).

[72] K.-K. Zhang, Z. Zhu, T. Shui, and W.-X. Yang, Generation of quantum entanglement and Einstein-Podolsky-Rosen steering in a hybrid qubit-cavity optomagnonic system, Chin. J. Phys. **92**, 284 (2024).

[73] X.-F. Pan, X.-L. Hei, X.-L. Dong, J.-Q. Chen, C.-P. Shen, H. Ali, and P.-B. Li, Enhanced spin-mechanical interaction with levitated micromagnets, Phys. Rev. A **107**, 023722 (2023).

[74] X.-L. Hei, X.-L. Dong, J.-Q. Chen, C.-P. Shen, Y.-F. Qiao, and P.-B. Li, Enhancing spin-photon coupling with a micromagnet, Phys. Rev. A **103**, 043706 (2021).

[75] W. Xiong, M. Tian, G.-Q. Zhang, and J. Q. You, Strong long-range spin-spin coupling via a Kerr magnon interface, Phys. Rev. B **105**, 245310 (2022).

[76] N. Benrass, A. Hidki, D. Aoune, and N. Habiballah, Enhancement of magnon-magnon entanglement in a double cavity-magnon system by optical parametric amplifier, Russ. Phys. J. **67**, 829 (2024).

[77] N. Benrass, A. Hidki, A. Lakhfif, D. Aoune, N. Habiballah, and M. Nassik, Quantifying entanglement by purity in a cavity-magnon system, Braz. J. Phys. **54**, 71 (2024).

[78] A. Hidki, A. Lakhfif, J. El Qars, and M. Nassik, Quantifying quantum correlations in a double cavity-magnon system, Eur. Phys. J. D **76**, 64 (2022).

[79] M. Moslehi, H. R. Baghshahi, M. J. Faghihi, and S. Y. Mirafzali, Entanglement between photonic and magnonic modes in an open optomagnonical system, Opt. Laser Technol. **168**, 109920 (2024).

[80] Y. Zhao, R. Zhao, L. Chen, J. Pan, and M. Zhang, Steady-state entanglement in a mechanically coupled double cavity containing magnetic spheres, Quantum Inf. Proc. **21**, 307 (2022).

[81] Q. Zheng, W. Zhong, G. Cheng, and A. Chen, Genuine magnon-photon-magnon tripartite entanglement in a cavity electromagnonical system based on squeezed-reservoir engineering, Quantum Inf. Proc. **22**, 140 (2023).

[82] J. Chen, X.-G. Fan, W. Xiong, D. Wang, and L. Ye, Nonreciprocal photon-phonon entanglement in Kerr-modified spinning cavity magnomechanics, Phys. Rev. A **109**, 043512 (2024).

[83] Z.-Y. Fan, L. Qiu, S. Gröblacher, and J. Li, Microwave-optics entanglement via cavity optomagnomechanics, Laser Photon. Rev. **17**, 2200866 (2023).

[84] A. Hidki, A. Lakhfif, N. Benrass, and M. Nassik, Entanglement enhancement through magnon squeezing and optical parametric amplifier in cavity magnomechanics, Chin. J. Phys. **90**, 319 (2024).

[85] A. Hidki, Y.-L. Ren, A. Lakhfif, J. El Qars, and M. Nassik, Enhanced maximum entanglement between two microwave fields in the cavity magnomechanics with an optical parametric amplifier, Phys. Lett. A **463**, 128667 (2023).

[86] A. Lakhfif, A. Hidki, A. Slaoui, and R. Ahl Laamara, Maximum enhancement of entanglement in cavity magnomechanics, Phys. Lett. A **518**, 129678 (2024).

[87] M.-C. Li, A.-X. Chen, and W. Zeng, Tripartite entanglement and entanglement transfer in a hybrid cavity magnomechanical system, Open Phys. **21**, 20220240 (2023).

[88] Z.-Q. Liu, Y. Liu, L. Tan, and W.-M. Liu, Reservoir engineering strong magnomechanical entanglement via dual-mode cooling, Ann. Phys. **535**, 2200660 (2023).

[89] A. Sohail, A. Hassan, R. Ahmed, and C.-S. Yu, Generation of enhanced entanglement of directly and indirectly coupled modes in a two-cavity magnomechanical system, Quantum Inf. Proc. **21**, 207 (2022).

[90] A. Sohail, R. Ahmed, R. Zainab, and C.-S. Yu, Enhanced entanglement and quantum steering of directly and indirectly coupled modes in a magnomechanical system, Phys. Scr. **97**, 075102 (2022).

[91] Q. Zheng, W. Zhong, G. Cheng, and A. Chen, Nonreciprocal microwave-optical entanglement in a magnon-based hybrid system, J. Appl. Phys. **135**, 084401 (2024).

[92] Q. Zheng, W. Zhong, G. Cheng, and A. Chen, Nonreciprocal macroscopic tripartite entanglement in atom-optomagnomechanical system, EPJ Quantum Technol. **11**, 8 (2024).

[93] S. Bayati, A. Mahdifar, and M. Bagheri Harouni, Entanglement formation between magnon and center-of-mass motion of a levitated particle in a magnomechanical system, Phys. Rev. A **110**, 013710 (2024).

[94] X.-L. Hei, P.-B. Li, X.-F. Pan, and F. Nori, Enhanced tripartite interactions in spin-magnon-mechanical hybrid systems, Phys. Rev. Lett. **130**, 073602 (2023).

[95] C. J. Foot, *Atomic Physics* (Oxford University Press, Oxford, 2004).

[96] J. Reichel and V. Vuletic, *Atom Chips* (Wiley, New York, 2011).

[97] J. Pérez-Ríos and Á. S. Sanz, How does a magnetic trap work?, Am. J. Phys. **81**, 836 (2013).

[98] C. Gonzalez-Ballestero, D. Hümmer, J. Gieseler, and O. Romero-Isart, Theory of quantum acoustomagnonics and acoustomechanics with a micromagnet, Phys. Rev. B **101**, 125404 (2020).

[99] W. Paul, Electromagnetic traps for charged and neutral particles, Rev. Mod. Phys. **62**, 531 (1990).
[100] S. Kolkowitz, A. C. B. Jayich, Q. P. Unterreithmeier, S. D. Bennett, P. Rabl, J. G. E. Harris, and M. D. Lukin, Coherent sensing of a mechanical resonator with a single-spin qubit, Science **335**, 1603 (2012).
[101] G. Adesso and F. Illuminati, Entanglement in continuous-variable systems: Recent advances and current perspectives, J. Phys. A: Math. Theor. **40**, 7821 (2007).
[102] A. Vinante, G. Wijts, O. Usenko, L. Schinkelshoek, and T. H. Oosterkamp, Magnetic resonance force microscopy of paramagnetic electron spins at millikelvin temperatures, Nat. Commun. **2**, 572 (2011).
[103] N. Shamsudhin, Y. Tao, J. Sort, B. Jang, C. L. Degen, B. J. Nelson, and S. Pané, Magnetometry of individual polycrystalline ferromagnetic nanowires, Small **12**, 6363 (2016).
[104] J. A. J. Burgess, A. E. Fraser, F. F. Sani, D. Vick, B. D. Hauer, J. P. Davis, and M. R. Freeman, Quantitative magnetomechanical detection and control of the Barkhausen effect, Science **339**, 1051 (2013).
[105] R. Fischer, D. P. McNally, C. Reetz, G. G. T. Assumpção, T. Knief, Y. Lin, and C. A. Regal, Spin detection with a micromechanical trampoline: Towards magnetic resonance microscopy harnessing cavity optomechanics, New J. Phys. **21**, 043049 (2019).
[106] H. M. Wiseman and G. J. Milburn, *Quantum Measurement and Control* (Cambridge University Press, Cambridge, England, 2009).
[107] G. Vidal and R. F. Werner, Computable measure of entanglement, Phys. Rev. A **65**, 032314 (2002).
[108] M. B. Plenio, Logarithmic negativity: A full entanglement monotone that is not convex, Phys. Rev. Lett. **95**, 090503 (2005).
[109] G. Adesso, A. Serafini, and F. Illuminati, Extremal entanglement and mixedness in continuous variable systems, Phys. Rev. A **70**, 022318 (2004).
[110] A. A. L. Rehaily and S. Bougouffa, Entanglement generation between two mechanical resonators in two optomechanical cavities, Intl. J. Theor. Phys. **56**, 1399 (2017).
[111] M. Yu, H. Shen, and J. Li, Magnetostrictively induced stationary entanglement between two microwave fields, Phys. Rev. Lett. **124**, 213604 (2020).
[112] M. Poot and H. S. van der Zant, Mechanical systems in the quantum regime, Phys. Rep. **511**, 273 (2012).
[113] M. Perdriat, C. Pellet-Mary, P. Huillery, L. Rondin, and G. Hétet, Spin-mechanics with nitrogen-vacancy centers and trapped particles, Micromachines **12**, 651 (2021).
[114] R. Simon, E. C. G. Sudarshan, and N. Mukunda, Gaussian pure states in quantum mechanics and the symplectic group, Phys. Rev. A **37**, 3028 (1988).
[115] R. Simon, N. Mukunda, and B. Dutta, Quantum-noise matrix for multimode systems: U(n) invariance, squeezing, and normal forms, Phys. Rev. A **49**, 1567 (1994).
[116] S. Olivares, Quantum optics in the phase space, Eur. Phys. J. Special Topics **203**, 3 (2012).
[117] K. Koga and N. Yamamoto, Dissipation-induced pure Gaussian state, Phys. Rev. A **85**, 022103 (2012).
[118] J. Gieseler, B. Deutsch, R. Quidant, and L. Novotny, Subkelvin parametric feedback cooling of a laser-trapped nanoparticle, Phys. Rev. Lett. **109**, 103603 (2012).
[119] P. Groszkowski, M. Koppenhöfer, H.-K. Lau, and A. A. Clerk, Reservoir-engineered spin squeezing: Macroscopic even-odd effects and hybrid-systems implementations, Phys. Rev. X **12**, 011015 (2022).
[120] H. Tan and J. Li, Einstein-Podolsky-Rosen entanglement and asymmetric steering between distant macroscopic mechanical and magnonic systems, Phys. Rev. Res. **3**, 013192 (2021).
[121] X. Zuo, Z.-Y. Fan, H. Qian, and J. Li, Entangling excitons with microcavity photons, Phys. Rev. Res. **6**, 023089 (2024).
[122] X. Zhang, C.-L. Zou, L. Jiang, and H. X. Tang, Cavity magnomechanics, Sci. Adv. **2**, e1501286 (2016).
[123] C. Gonzalez-Ballestero, J. Gieseler, and O. Romero-Isart, Quantum acoustomechanics with a micromagnet, Phys. Rev. Lett. **124**, 093602 (2020).
[124] J. Gieseler, L. Novotny, and R. Quidant, Thermal nonlinearities in a nanomechanical oscillator, Nat. Phys. **9**, 806 (2013).
[125] A. H. Ghadimi, S. A. Fedorov, N. J. Engelsen, M. J. Bereyhi, R. Schilling, D. J. Wilson, and T. J. Kippenberg, Elastic strain engineering for ultralow mechanical dissipation, Science **360**, 764 (2018).
[126] D. Mason, J. Chen, M. Rossi, Y. Tsaturyan, and A. Schliesser, Continuous force and displacement measurement below the standard quantum limit, Nat. Phys. **15**, 745 (2019).
[127] R.-C. Shen, J. Li, Y.-M. Sun, W.-J. Wu, X. Zuo, Y.-P. Wang, S.-Y. Zhu, and J. Q. You, Cavity-magnon polaritons strongly coupled to phonons, Nat. Commun. **16**, 5652 (2025).
[128] Y. Tabuchi, S. Ishino, T. Ishikawa, R. Yamazaki, K. Usami, and Y. Nakamura, Hybridizing ferromagnetic magnons and microwave photons in the quantum limit, Phys. Rev. Lett. **113**, 083603 (2014).
[129] H. Maier-Flaig, S. Klingler, C. Dubs, O. Surzhenko, R. Gross, M. Weiler, H. Huebl, and S. T. B. Goennenwein, Temperature-dependent magnetic damping of yttrium iron garnet spheres, Phys. Rev. B **95**, 214423 (2017).
[130] S. Klingler, H. Maier-Flaig, C. Dubs, O. Surzhenko, R. Gross, H. Huebl, S. T. B. Goennenwein, and M. Weiler, Gilbert damping of magnetostatic modes in a yttrium iron garnet sphere, Appl. Phys. Lett. **110**, 092409 (2017).
[131] R. L. White and I. H. Solt, Multiple ferromagnetic resonance in ferrite spheres, Phys. Rev. **104**, 56 (1956).
[132] S. Kosen, A. F. van Loo, D. A. Bozhko, L. Mihalceanu, and A. D. Karenowska, Microwave magnon damping in YIG films at millikelvin temperatures, APL Mater. **7**, 101120 (2019).